

Figure 10. Parameter setting analysis. We test extensive settings of the three parameters in our framework on the FAUST dataset, including the number of the scales L , the first k eigenvectors, eigenvalues used and the iteration times, where each case with one parameter varied and the other remaining the same. The corresponding average geodesic errors and average runtime are shown in each subfigure.

A. Proof of Remark 4.1

As we know, since the tight wavelet frame has $G(\lambda) = \sum_s g^2(s\lambda) \equiv 1, \lambda \in [0, \lambda_{\max}]$, we get $\sum_s g^2(s\Lambda) = \mathbf{I}$, where \mathbf{I} is an identity matrix. According to (6), i.e. If we let

$$\mathbf{C}g(s\Lambda_{\mathcal{M}})\Phi_{\mathcal{M}}^+ = g(s\Lambda_{\mathcal{N}})\Phi_{\mathcal{N}}^+\mathbf{P}^T, \forall s,$$

from the the orthogonality of the eigenvectors of the LBO $\Phi_{\mathcal{M}}^+\Phi_{\mathcal{M}} = \mathbf{I}$, where \mathbf{I} is an identity matrix, we have

$$\begin{aligned} \mathbf{C}g(s\Lambda_{\mathcal{M}}) &= g(s\Lambda_{\mathcal{N}})\Phi_{\mathcal{N}}^+\mathbf{P}^T\Phi_{\mathcal{M}}, \forall s \\ \mathbf{C}g^2(s\Lambda_{\mathcal{M}}) &= g(s\Lambda_{\mathcal{N}})\Phi_{\mathcal{N}}^+\mathbf{P}^T\Phi_{\mathcal{M}}g(s\Lambda_{\mathcal{M}}), \forall s, \\ \sum_s \mathbf{C}g^2(s\Lambda_{\mathcal{M}}) &= \sum_s g(s\Lambda_{\mathcal{N}})\Phi_{\mathcal{N}}^+\mathbf{P}^T\Phi_{\mathcal{M}}g(s\Lambda_{\mathcal{M}}), \\ \mathbf{C}\sum_s g^2(s\Lambda_{\mathcal{M}}) &= \sum_s g(s\Lambda_{\mathcal{N}})\Phi_{\mathcal{N}}^+\mathbf{P}^T\Phi_{\mathcal{M}}g(s\Lambda_{\mathcal{M}}). \end{aligned}$$

We finally get

$$\mathbf{C} = \sum_s g(s\Lambda_{\mathcal{N}})\Phi_{\mathcal{N}}^+\mathbf{P}^T\Phi_{\mathcal{M}}g(s\Lambda_{\mathcal{M}}).$$

B. Additional materials

Parameter analysis. We intend to find the relative optimal settings of three important parameters in our framework via extensive experiments, containing the discrete scales $L + 1$, iteration times and the first k eigenvalues and eigenvectors used. All matching results under various parameter settings are detailedly shown in Figure 10. We can find that the performance improvements become less sensitive to the increase of L if $L + 1 > 4$. A similar occasion also

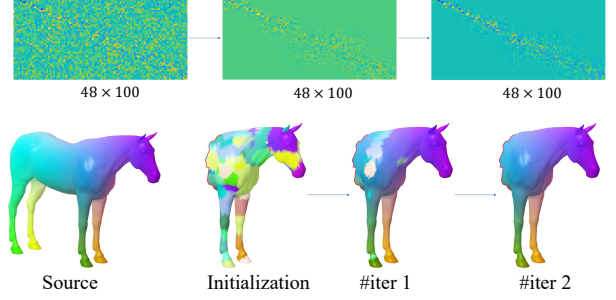


Figure 11. Demonstration of partial shape correspondence. Starting with a noisy functional map, we alternately optimize the functional maps and the pointwise maps. The pointwise maps are visualized by color transfer. The functional map matrix \mathbf{C} has a slanted-diagonal structure for partial shape correspondence.

happens to k when $k > 100$. However, as opposed to the non-significant improvement of the performance, the computing time has increased dramatically when k continuously increases. Thus, to balance the performance and the computation efficiency well, we generally set $k = 100$ and $L = 5$ in the following experiments. Remarkably, Figure 10 also shows that our method tends to be stable within three or four iterations. This allows us to generally take 3 iterations in all following experiments.

Details on partial shape correspondence. The core idea is the spectral manifold wavelets (SMWs) inheriting the isometric invariance of the Laplace-Beltrami eigenfunctions. However, on partial shapes, this invariance has been broken down, as the removal of shape parts changes the Laplace-Beltrami eigenfunctions. To recover the partial isometries, we truncate the Laplace-Beltrami eigenfunctions with different sizes, in order to enforce the expectation of a slanted diagonal by allowing rectangular \mathbf{C} . This technique is feasible, since the PFM [29] has shown the functional map has a slanted diagonal structure proportional to the surface area. A demonstration of partial shape correspondence of our method is shown in Figure 11. We will release the implementation of our method upon publication. For more details about how to truncate the Laplace-Beltrami eigenfunctions in partial shape correspondence, please refer to the PFM [29] and ZoomOut [19].